Plasma Sci. Technol. **26** (2024) 125104 (10pp) https://doi.org/10.1088/2058-6272/ad79b0

Equilibrium reconstruction method for self-organized plasmas on reversed field pinches with polarimeter-interferometer

Yuhua HUANG (黄玉华)[1], **Ke LIU** (刘珂)[1], **Wenzhe MAO** (毛文哲)[1,*], **Caoxiang ZHU** (祝曹祥)[1,*], **Tao LAN** (兰涛)[1], **Yiming ZU** (祖一鸣)[2], **Yongkang ZHOU** (周永康)[1], **Xingkang WANG** (汪兴康)[1], **Peng DENG** (邓鹏)[1], **Li WANG** (王立)[1], **Pai PENG** (彭湃)[1], **Adi LIU** (刘阿娣)[1], **Chu ZHOU** (周楚)[1], **Haifeng LIU** (刘海峰)[3], **Hong LI** (李弘)[1], **Jinlin XIE** (谢锦林)[1], **Yuhong XU** (许宇鸿)[3], **Weixing DING** (丁卫星)[1], **Wandong LIU** (刘万东)[1] **and Ge ZHUANG** (庄革)[1]

[1] School of Nuclear Science and Technology, University of Science and Technology of China, Hefei 230026, People's Republic of China
[2] Institute for Fusion Theory and Simulation, Department of Physics, Zhejiang University, Hangzhou 310027, People's Republic of China
[3] School of Physical Science and Technology, Southwest Jiaotong University, Chengdu 610031, People's Republic of China

[*]E-mail of corresponding authors: maozhe@ustc.edu.cn and caoxiangzhu@ustc.edu.cn

Received 20 March 2024, revised 9 September 2024
Accepted for publication 11 September 2024
Published 8 November 2024

Abstract
In the reversed field pinch (RFP), plasmas exhibit various self-organized states. Among these, the three-dimensional (3D) helical state known as the "quasi-single-helical" (QSH) state enhances RFP confinement. However, accurately describing the equilibrium is challenging due to the presence of 3D structures, magnetic islands, and chaotic regions. It is difficult to obtain a balance between the available diagnostic and the real equilibrium structure. To address this issue, we introduce KTX3DFit, a new 3D equilibrium reconstruction code specifically designed for the Keda Torus eXperiment (KTX) RFP. KTX3DFit utilizes the stepped-pressure equilibrium code (SPEC) to compute 3D equilibria and uses polarimetric interferometer signals from experiments. KTX3DFit is able to reconstruct equilibria in various states, including axisymmetric, double-axis helical (DAx), and single-helical-axis (SHAx) states. Notably, this study marks the first integration of the SPEC code with internal magnetic field data for equilibrium reconstruction and could be used for other 3D configurations.

Keywords: equilibrium reconstruction, polarimeter-interferometer, multi-region relaxed MHD, 3D self-organized states, reversed field pinch

(Some figures may appear in colour only in the online journal)

1. Introduction

High-beta plasmas in axisymmetric devices, like tokamaks and reversed field pinches, may become non-axisymmetric under the increasing magnetic fluctuation, indicating that the three-dimensional (3D) effects of the magnetic topology may play a crucial role in confinement [1–3]. The magnetic configuration in the reversed field pinch (RFP) is characterized by high plasma beta, rich MHD instability modes, and significant changes in magnetic topology due to 3D effects [4, 5]. Therefore, RFP is an excellent platform for conducting systematic experimental investigations into 3D physics

[*] Authors to whom any correspondence should be addressed.

issues in magnetic confinement fusion devices.

In typical RFP plasmas, a series of tearing modes exist with poloidal mode numbers $m = 0$ and $m = 1$, each associated with different toroidal mode numbers [6, 7]. As these tearing modes grow and reach a certain size, magnetic islands overlap and the magnetic field becomes stochastic [8, 9]. Large stochastic regions result in relatively flat density and temperature profiles in the plasma core. Consequently, the overall confinement level in RFP is restrained [10]. In RFP, this state, characterized by multiple coexisting helical modes and relatively poor confinement performance, is typically referred to as the multiple helicity (MH) state. The "quasi-single-helical" (QSH) state, which has been observed in several RFP devices, can significantly improve the confinement in RFP [6, 11–13]. Therefore, studying the 3D physical characteristics of QSH states is of great importance for understanding how to improve RFP performance.

The QSH state features a dominant mode with $m = 1$ and multiple weaker secondary unstable modes, resulting in higher core plasma temperatures and improved energy confinement performance [11–13]. From the perspective of magnetic topologies, the QSH state can be classified into two categories: double-axis helical (DAx) state and single-helical-axis (SHAx) state [12]. The generation of the QSH state arises from the self-organized behavior of the plasma [4], but the mechanism of transition processes among MH state, DAx state, and SHAx state is not fully understood. Experimental investigations into the formation, transformation, and maintaining of 3D self-organized plasmas are required for better understanding of the physical nature of RFP plasmas and enhancing control techniques for self-organized states.

Equilibrium profiles are usually required to further study instabilities and transport in fusion plasmas. Since it is impossible to measure every quantities in the whole plasma, a common technique is to reconstruct the equilibrium state using limited measured data. For axisymmetric plasmas, the equilibrium can be described by the Grad-Shafranov equation, which is used by various reconstruction codes, such as EFIT [14, 15], CLISTE [16], LIUQE [17], and NICE [18]. In the case of 3D equilibrium reconstruction problems, complete equilibrium equations need to be solved. A typical way is to minimize the energy functional derived from ideal MHD equations. Following this idea, 3D equilibrium code VMEC was developed [19, 20] and later it was used in the equilibrium reconstruction tool V3FIT [21]. While both VMEC and V3FIT were initially developed for stellarators, they have been successfully applied to RFP and tokamak devices [22, 23]. The axisymmetric equilibrium codes and VMEC are all assuming continuously nested magnetic surfaces, so the reconstructed equilibrium has no island or stochastic regions. 3D equilibrium reconstruction can be also achieved by adding the solution of tearing mode eigenvalues to an axisymmetric equilibrium [24, 25]. The procedure involves achieving an initial axisymmetric equilibrium result, followed by solving a series of Newcomb's equation [26] for magnetic perturbations in the toroidal geometry. Then, the axisymmetric equilibrium is superimposed with the magnetic perturbations to reconstruct the QSH state [25, 27]. Although magnetic islands are captured in this method, it is not a non-linear approach and the final equilibrium is a superposition of a secular part and a perturbation.

There is a new MHD model, multi-region relaxed magnetohydrodynamic (MRxMHD) [28–30], which represents an extented application of Taylor's theory [31, 32]. This model involves independently solving force-free equilibrium equations in various regions, with constrains ensuring force balance across different regions. This model does not assume nested magnetic surfaces, allowing it to describe important magnetic structures such as magnetic islands and chaotic magnetic field regions. The stepped-pressure equilibrium code (SPEC), which is developed based on the MRxMHD model, has been used to study various equilibrium states in RFP [33, 34].

For equilibrium reconstructions, it is crucial that the experimental diagnostic methods are directly related to the magnetic field to the greatest extent possible. However, it is not only the number of experimental constraints that improves the solution, but also the quality of these constraints. Having only external magnetics measurements, regardless of their number, does not provide the same information as internal measurements. The polarimeter-interferometer [35], capable of measuring core data, is an excellent diagnostic tool for the reconstruction process [36]. It can non-perturbatively measure the core magnetic field and density with high temporal resolutions. Additionally, it can simultaneously measure the equilibrium and fluctuation quantities for both the magnetic field and density. The equilibrium and fluctuation quantities can be used for equilibrium reconstruction and instability studies [37], respectively.

In this paper, we introduce a new code, KTX3DFit, which can reconstructed different 3D plasma states with the magnetic islands and stochastic regions in RFP.

This paper is organized as follows. We begin with an introduction to the theoretical framework of the MRxMHD model, and provide different 3D self-organized states based on the theory in KTX. Details of the simulation of polarimeter-interferometer signals are presented in section 3, where the plasma equilibrium comes from the section 2. The approach and results of the equilibrium reconstruction of 3D self-organized states are presented in section 4. The concluding remarks and discussions are presented in section 5.

2. The MRxMHD model and equilibrium simulations of 3D self-organized states

2.1. Multi-region relaxed MHD model

According to Taylor's theory, the final state reached by the plasma after relaxation is a minimum-energy state with helicity constraint [31, 32]. The MRxMHD model [28, 29] extends the application of Taylor's theory. The entire space can be divided into several subvolumes using multiple interfaces, which are preserved as transport barriers [33]. A set of nested toroidal interfaces, denoted as I_i, where $i = 1,2,\ldots,N_v$ and N_v is the number of subvolumes. The subvolume V_i is the annular volume enclosed by I_{i-1} and I_i. Each subvolume has a local energy W_i defined as [28]

$$W_i = \int_{V_i} \left(\frac{B^2}{2\mu_0} + \frac{p_i}{\gamma - 1} \right) \mathrm{d}V_i, \tag{1}$$

where p_i is stepped pressure, and γ is the adiabatic index. When the helicity K_i is invariant in each subvolume, the energy functional F_i for the MRxMHD model is given by

$$F_i = \sum_{i=1}^{N_v} \cdot \left(W_i - \frac{\mu_i}{2} \left(\int_{V_i} \cdot \boldsymbol{A} \cdot \boldsymbol{B} \mathrm{d}V_i - K_i \right) \right), \tag{2}$$

where μ_i is the Lagrange multiplier. The variation of the energy functional with respect to the variation in magnetic field $\delta \boldsymbol{B} = \nabla \times \delta \boldsymbol{A}$ and perturbation displacement ξ is [28, 38]

$$\delta F_i = \int_{V_i} (\nabla \times \boldsymbol{B} - \mu_i \boldsymbol{B}) \cdot \delta \boldsymbol{A} \mathrm{d}V_i - \int_{\partial V_i} \left(p_i + \frac{B^2}{2\mu_0} \right) \xi \cdot \mathrm{d}\boldsymbol{s}. \tag{3}$$

When the functional is extremal, $\delta F_i = 0$, the Beltrami equation [30] is satisfied within each subvolume,

$$\nabla \times \boldsymbol{B} = \mu_i \boldsymbol{B}. \tag{4}$$

Simultaneously, ensuring that the total pressure is equal on both sides of each interface,

$$\left[\left[p_i + \frac{B^2}{2\mu_0} \right] \right]_{I_i} = 0, \tag{5}$$

where the bracket $[[*]]$ indicates the jump of the scalar across interface I_i.

The SPEC [28, 39, 40] serves as a numerical solver for the MRxMHD model [29, 30]. The total pressure passing through interface I_i always satisfies equation (5). The pressure gradient ∇p is zero in each subvolume, resulting in a stepped distribution of the overall pressure. SPEC iteratively adjusts the interface shapes to solve for the magnetic field within each subvolume V_i, until the total pressure passing through interface I_i reaches equilibrium.

2.2. Equilibrium simulation of 3D self-organized states in KTX

This section uses the SPEC code [28] to simulate the 3D equilibrium with KTX configuration. In the QSH state, a transport barrier is present, with significant differences in physical properties observed on either side of the barrier [41–43]. We employed an interface as a transport barrier to divide the plasma region into two subvolumes in our simulation [33, 34]. QSH state with a toroidal field periodicity [43, 44] $N_\mathrm{p} = 6$ is expected to stably achieve by the negative magnetic shear in the future KTX experiments [45]. The input data [34] are the toroidal field periodicity N_p ($N_\mathrm{p} = 6$ [45]), toroidal flux ψ_i, stepped pressure p_i and helicity K_i, where $i = 1,2$ represent the inner and outer subvolume, respectively. The difference between the two stepped-pressures is set to $p_1 - p_2 = 560$ Pa and the total toroidal flux is $\psi = \psi_1 + \psi_2 = 0.1298$ Wb according to the design parameters of KTX. The step of the pressure profile is determined by the magnetic flux of the subvolume. The transport barrier locates at a relatively outer position in the radial direction. The flux of inner subvolume is $\psi_1 = 0.86\psi$, which keeps the position of the interface relatively out. The SPEC outputs are the shape of the interface and the vector potential $\boldsymbol{A}$. The magnetic field can be obtained by solving $\boldsymbol{B} = \nabla \times \boldsymbol{A}$ in SPEC and choosing an appropriate interface shape to balance the total pressure across I_i.

We achieved plasma equilibrium by scanning the helicity [34]. By fixing the helicity in the boundary subvolume and increasing the helicity in the core region, the transition of the plasma from axisymmetric state to the DAx state and finally to the SHAx state was achieved, as depicted in figure 1. The magnetic field for each self-organized state in figure 1 represents the minimum energy state with constant helicity in each subvolume. In conclusion, the MRxMHD model and SPEC indeed possess the capability to achieve 3D self-organized equilibrium in KTX. Moreover, the results in this section can provide data support for sections 3.2 and 4.2.

3. Simulation diagnosis of polarimeter-interferometer in self-organized states

3.1. Introduction to polarimeter-interferometer

Our goal is to develop a program for reconstructing the 3D self-organized plasma equilibrium in RFP based on the

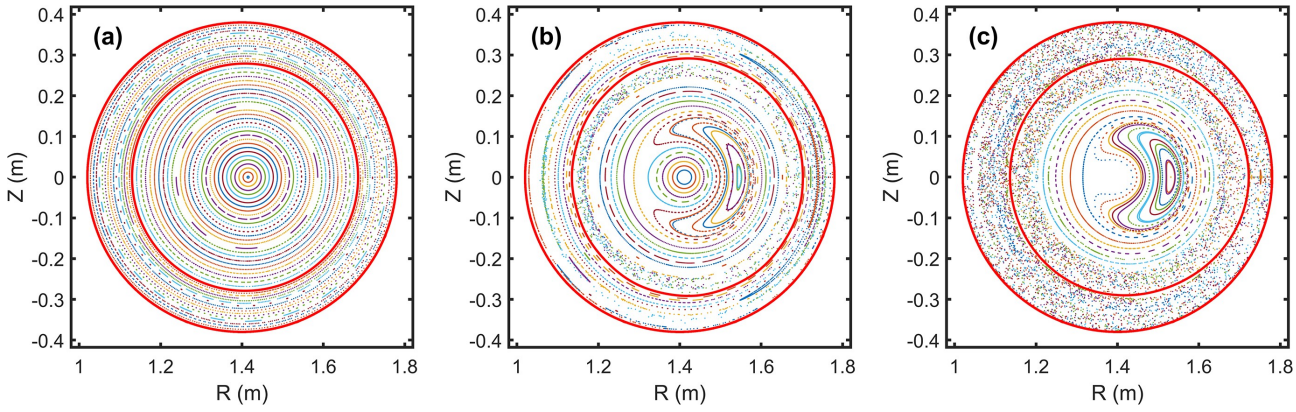

Figure 1. Poincare cross sections at $\zeta = 0°$ of magnetic field in different self-organized states are presented. (a) Axisymmetric state, (b) DAx state, (c) SHAx state. The thick red contours denote the ideal interface.

SPEC code, using experimental diagnostic data as constraint conditions. As the helical structure of the QSH state is situated in the core, utilizing a diagnostic capable of detecting the core plasma parameters could provide the most effective information for equilibrium reconstruction. The polarimeter-interferometer [35] is chosen to be the main data sources, since it enables absolute measurements of the magnetic field, encompassing both equilibrium and fluctuation components [46, 47]. It also achieves high temporal resolution with adjustable intermediate frequency. Spatial resolution can also be improved by manipulating positions and channels of diagnostic beams. Moreover, the polarimeter-interferometer, can provide distribution information of density and magnetic field synchronously.

A linearly polarized light beam can be injected vertically into magnetized plasma of KTX [48], and the polarization direction rotates because of faraday rotation effect, which also causes phase shift received by the detector. Phase difference ϕ can be expressed as [46]

$$\phi_{(x)} = 2.62\times10^{-13}\lambda^2\int B_z(x,z)n_e(x,z)\mathrm{d}z, \tag{6}$$

where B_z is the component of the magnetic field along the beam direction, n_e is the electron density, x indicates the radial position of incident light, z represents the coordinate along the optical path direction, and λ is the wavelength of the laser. Generally, the position of the interferometer channel and polarimeter channel is the same, and so is the length of beam path across plasma. Therefore, n_e in equation (6) is obtained synchronously with the interferometer. The interferometer offers density signals integrated along the chord of the optical path [46],

$$\int n_e\mathrm{d}l = \int n_e(x,z)\mathrm{d}z. \tag{7}$$

In experiments as the polarimeter-interferometer provides chord-integrated value, obtaining localized information from the diagnostic data requires employing specific inversion techniques. The Abel inversion [49], in conjunction with equation (7), can be employed to determine the density distribution $n_e(x,z)$ required in equation (6).

3.2. Simulation of polarimeter-interferometer signals in the KTX self-organized states

This work in this section enables the evaluation and validation of the polarimeter-interferometer's capability to measure the QSH state on KTX. It also serves as a prior reference for future experimental data analysis. Moreover, the forward process of calculating the polarimeter-interferometer signals under different states enables the assessment of feasibility of using polarimeter-interferometer for the inversion and reconstruction of the 3D self-organized equilibrium states.

The input data for the simulation in this section are λ, $B_z(x,z)$ and $n_e(x,z)$. $\lambda = 432.5\times10^{-6}$ m. According to equations (6) and (7), the data for $B_z(x,z)$ are derived from the equilibrium results of each self-organized state achieved in section 2.2. However, the equilibrium results do not include density information. Previous studies have indicated that the ratio of core to edge density in RFP plasma is typically around $2-1$ [50]. In large magnetic confinement fusion devices, the chord-integrated electron density is usually above 1×10^{19} m^{-2}, and the multi-channel terahertz solid interferometer system already installed on the KTX device can also exhibit chord-integrated densities above 1×10^{19} m^{-2} [51]. For simplicity in this work, the density in the core and edge regions of the plasma is set to $\frac{n_e^{\mathrm{core}}}{n_e^{\mathrm{edge}}} = 2$, where $n_e^{\mathrm{core}} = 2\times10^{19}$ m^{-2} and $n_e^{\mathrm{edge}} = 1\times10^{19}$ m^{-2}. The core and edge regions are separated by the interface. Additionally, the same density model is assumed for each self-organized state. Under the assumption of magnetic freezing, the specific distribution of density is related to the distribution of magnetic field lines. The signals of chord-integrated density and Faraday rotation angle in this section are calculated based on equations (6) and (7), along with the aforementioned density model, where the plasma equilibrium comes from section 2.2.

The polarimeter-interferometer on KTX consists of 3 channels, all oriented vertically and radially concentrated in the core region [48], as shown in figure 2(a). Their radial positions are at R = 1.34 m, 1.4 m, and 1.46 m, respectively, where R is the major radius. Moreover, The phase noises of the polarimeter and interferometer are less than 0.8° and 0.9° [48], respectively. Figures 3(a) and (b) present the simulated signals from the 3-channel polarimeter-interferometer under different self-organized states acquired from section 2.2. Figures 3(a) and (b) can provide partial information about the ideal 3D structure. However, the evolution of the plasma from the DAx state to the SHAx state may involve smaller-scale magnetic island structures (figures 3(a) and (b)), necessitating an augmentation in the number of polarimeter-interferometer channels to achieve higher spatial resolution.

The minor radius of KTX is 0.4 m, and 21 vertical beam lines (figure 2(b)) go through the plasma volume if placed at radial intervals of 3.6 cm (with tighter spacing in the core), which is approaching the diameter of diagnostic window. On the other hand, this beam waist is about 2 cm to avoid crosstalk. To explore the impact of the number of polarime-

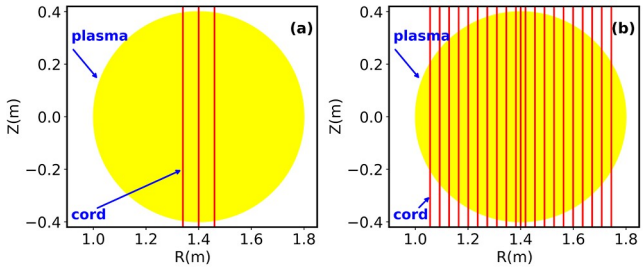

Figure 2. The polarimeter-interferometer layout for the KTX cross-section. (a) 3-channel polarimeter-interferometer on the KTX experimental device, and (b) the hypothetical 21-channel layout proposed to improve the resolution of the polarimeter-interferometer in this simulation.

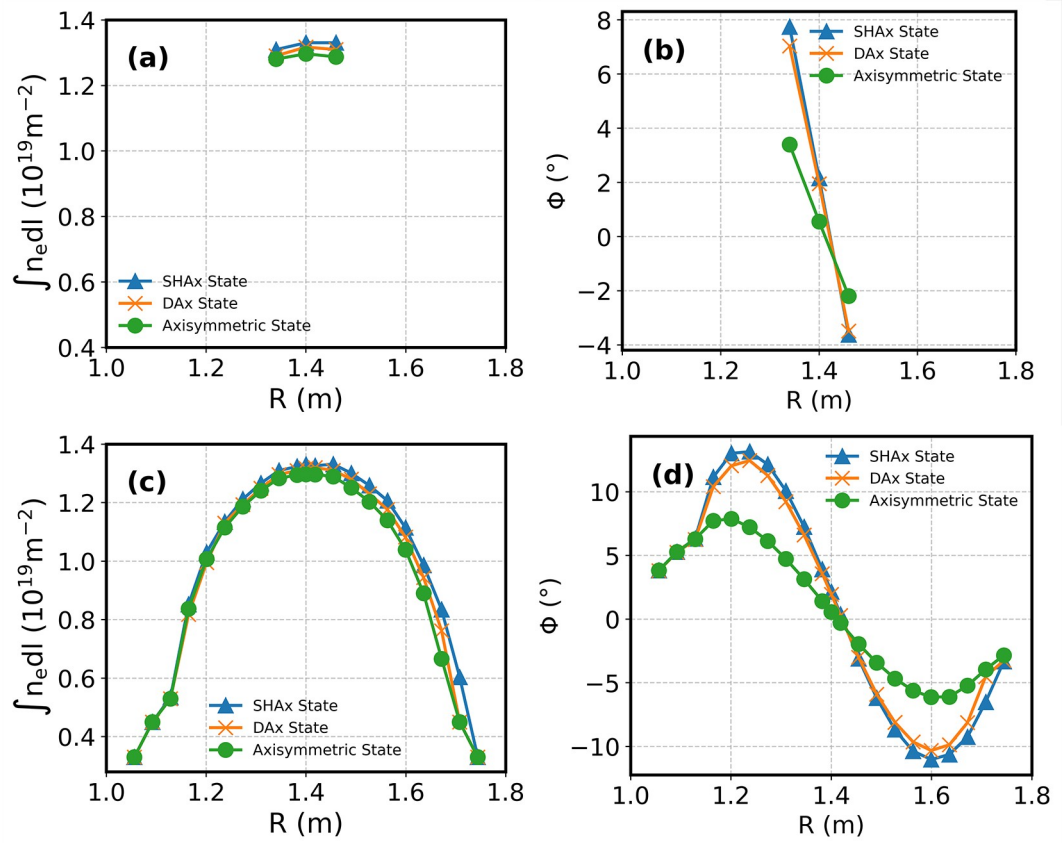

Figure 3. The polarimeter-interferometer signals of different self-organized states at $\zeta = 0°$ in KTX are displayed for both 3-channels and 21-channels, where ζ is toroidal angle. (a) and (c) depict chord-integrated density signals, while (b) and (d) show Faraday rotation angle signals.

ter channels and the response sensitivity of position to the 3D structure, we set the maximum number of beam channels to 21 in this simulation, as depicted in figure 2(b). Figures 3(c) and (d) illustrate discernible differences in the polarimeter-interferometer signals for different self-organized states at the same toroidal position. The additional channels enable a more comprehensive presentation of the signals, better satisfying the requirements for inversion and reconstruction. As shown in figure 3(d), due to the change in the poloidal field direction, the sign of the Faraday rotation angle is opposite on either side of the magnetic axis. The position of the magnetic axis can be determined based on where the Faraday rotation angle is equal to zero. In the toroidal geometry, the variation trend of the faraday rotation signal in the radial direction is foreseeable.

In cases where the amplitude of the 3D magnetic field components is weak, experimentally, we can distinguish the magnetic helical structure by employing diagnostics at multiple toroidal positions. However, in the experiments, the polarimeter-interferometer is typically constructed at a single toroidal location. Based on the 3D structure rotates with plasma, we expect to observe periodic temporal oscillations in the signals. Taking the toroidal position at $\zeta = 0°$ as an example, in a specific equilibrium state from the equilibrium program, helical plasma at different toroidal positions rotates across the measurement point at $\zeta = 0°$. As a result, in our simulation, the polarimeter-interferometer signals from various toroidal positions are expressed as signals at different times, as depicted in figure 4. Figure 4 shows that a single-channel polarimeter-interferometer can display signal intensity differences over time during transitions between various states.

Subsequently, we select four different toroidal positions within one toroidal periodicity to simulate the polarimeter-interferometer signals of 21 channels under different self-organized states, as illustrates in figure 5. We observe significant differences between the signals of axisymmetric states and QSH states at various toroidal positions. Due to $N_p = 6$, the poloidal direction will rotate one full revolution at $\zeta = 60°$. Along the toroidal direction, the DAx and SHAx states exhibit helical structures, representing 3D configurations, which lead to variations in the signals at different toroidal positions. Due to the distinct magnetic topologies of SHAx and DAx states, their signals also differ. It is foreseeable that the signals at different toroidal positions under axisymmetric and other 2D structures will be identical. Therefore, it is evident that positioning the polarimeter-interferometer at different toroidal positions and increasing the radial coverage can help to identify different equilibrium states during their transitions.

From the above, signals from different self-organized states at the same toroidal position, along with the variations in signals at different toroidal positions for each self-organized state, and the simulated temporal signals of a single-

channel polarimeter-interferometer at a specific toroidal position, all indicate the responsiveness of the polarimeter-interferometer to different self-organized states. Consequently, simulation results indicate that increasing beam channels at different toroidal and horizontal positions can provide better spatial resolution to help accomplish the equilibrium reconstruction of self-organized states during the transition among different states. Furthermore, distribution of channels with different poloidal positions and incident angle may also affect the reconstruction, which is not included in the scope of this study.

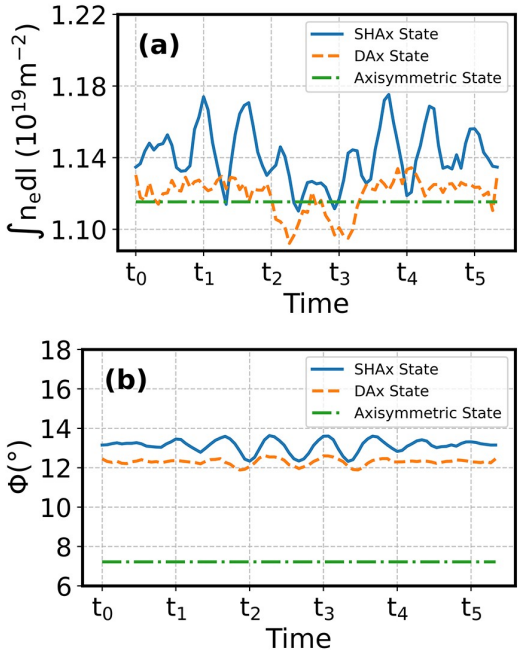

Figure 4. The simulated temporal signals of a single-channel polarimeter-interferometer at $\zeta = 0°$, $R = 1.24$ m for different self-organized states. (a) Chord-integrated density and (b) the Faraday rotation angle.

4. KTX3DFit: reconstructing 3D self-organized states in KTX

The simulation of polarimeter-interferometer signals based on the plasma equilibrium calculated by SPEC is a forward process, also known as the forward problem [52]. Determining the overall parameters using experimentally observed signals is referred to as the inverse problem. The inverse problem involves inferring initial parameters that match the measured integrated or boundary values obtained from experimental measurements on an existing theoretical model. Its aim is to obtain specific distributions of the targets of interest. The equilibrium reconstruction code named KTX3DFit has been developed for 3D plasma studies based on this strategy. In KTX3DFit, SPEC serves as the numerical solver in the forward process. By employing polarimeter-interferometer constraints, the process of solving the inverse problem in the new code determines the free parameters in the numerical model of SPEC, corresponding to a solution of plasma equilibrium.

The primary input data in the KTX3DFit are stepped pressure p_i ($p_1 - p_2 = 560$ Pa), toroidal field periodicity $N_p = 6$ [45], the reference Faraday rotation angle ϕ^{ref}, and initialized 5 free parameters, where the 5 free parameters are magnetic flux $\psi_{t,1}$ and helicity κ_1 in the core region, and toroidal magnetic flux $\psi_{t,2}$, poloidal magnetic flux $\psi_{p,2}$, and helicity κ_2 in the boundary region [33]. To avoid confusion, we emphasize the differences between the inputs for

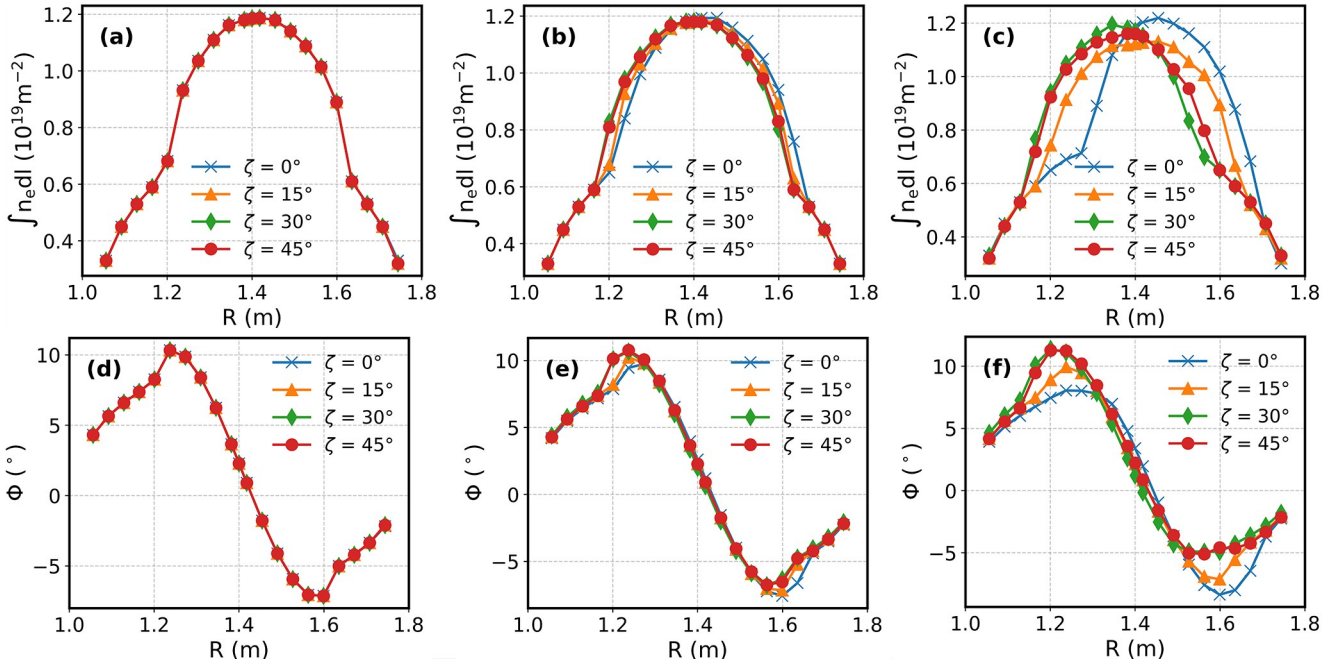

Figure 5. Polarimeter-interferometer signals for different self-organized states at various toroidal positions: (a) and (d) for axisymmetric state, (b) and (e) for DAx state, (c) and (f) for SHAx state, showing chord-integrated density and Faraday rotation angle signals, respectively.

KTX3DFit and those in section 2.2. Here, the 5 free parameters are primarily calculated automatically using the quasi-Newton algorithm within KTX3DFit. In contrast, in section 2.2, the magnetic flux is specified, and helicity values are scanned within a specific range. Moreover, the output of KTX3DFit is the reconstructed equilibrium.

In order to verify the correctness of our inversion results, we need a reference value. This reference signal can be obtained from measurements or any numerical tools. It is worth noting that due to the lack of measurement data for different states, section 4.2 uses numerical tools, such as VMEC [20] or SPEC, to obtain ϕ^{ref}, which are not from the measurements.

4.1. Equilibrium reconstruction code KTX3DFit

Let us first introduce the cost function (equation (8)) used in the KTX3DFit. In equilibrium inversion calculations, D_j is used to represent the calculation values using given equilibrium state, and M_j represents the experimental diagnostic measurements. The parameter χ^2 is used to characterize the disparity between D_j and M_j [14, 25].

$$\chi^2 = \sum_j \frac{(D_j - M_j)^2}{\sigma_j^2}, \tag{8}$$

where σ_j represents the level of error in experimental data. The idea of KTX3DFit is explicit: to find the best fit of equilibrium model with experimental data by minimizing χ^2. KTX3DFit adopts the Quasi-Newton algorithm for minimization.

Next, the specific setting of the cost function in this study will be presented. It was demonstrated that SHAx state and DAx state can be reproduced with only 5 parameters in a minimal constraint equilibrium model [33]. In this model, the 5 constraints for the equilibrium of MRxMHD plasma in two subregions involves the $\psi_{\mathrm{t},1}$, κ_1, $\psi_{\mathrm{t},2}$, $\psi_{\mathrm{p},2}$, κ_2. To test the capability of KTX3DFit, we adopt similar settings with 2 regions and 5 free parameters, referred to as the degrees of freedom f, i.e., $f = \{\psi_{\mathrm{t},1}, \kappa_1, \psi_{\mathrm{t},2}, \psi_{\mathrm{p},2}, \kappa_2\}$. KTX3DFit's primary task is to identify f in the equilibrium model. In accordance with the feasibility analysis of reconstruction using polarimeter-interferometer signals as constraints in section 3.2, we use the same radial positions in figure 2(b), distributed at the toroidal angles $\zeta = 0°$, 15°, 30°, 45°. According to equation (8), we have

$$\chi^2 = \sum_{N_\zeta=1}^{4} \sum_{j=1}^{21} \frac{(\phi_j^{\mathrm{calculate}} - \phi_j^{\mathrm{ref}})^2}{M\sigma_j^2}, \tag{9}$$

where ϕ_j^{ref} is defined as reference signal in this study detailed in section 4.2. $\phi_j^{\mathrm{calculate}}$ represents the Faraday rotation angle signals in the polarimeter-interferometer, originating from equilibrium reconstruction data. Additionally, $\phi_j^{\mathrm{calculate}}$ is a function of the free parameters f, i.e., $\phi_j^{\mathrm{calculate}} = \phi_j(f) = \phi_j(\psi_{\mathrm{t},1}, \kappa_1, \psi_{\mathrm{t},2}, \psi_{\mathrm{p},2}, \kappa_2)$. j denotes the index of the polarimeter-interferometer channel, N_ζ is the number of toroidal positions and M represents the weight . For convenience in this work, we set M to 1. The measurement error consists of both systematic and random components. Systematic error mainly refers to the noise level. The cost function considers systematic error (noise) as error, referencing the KTX polarimeter-interferometer system [48]. So, the error σ_j represents the noise in the polarimeter-interferometer signal, with $\sigma_j = 0.8°$.

Finally, the workflow of KTX3DFit will be outlined. KTX3DFit begins by initializing parameters f, employs SPEC to attain plasma equilibrium, and then, based on these equilibria, calculates the polarization-interferometer signals $\phi_j^{\mathrm{calculate}}$. Subsequently, it integrates polarimeter-interferometer measurements as constraints and minimizes χ^2. During the process of minimizing χ^2, KTX3DFit employs the quasi-Newton algorithm to automatically calculate free parameter f within the equilibrium model. This loop allows the program to interatively cycle until convergence is achieved. KTX3DFit returns the values of f, and reconstructed magnetic equilibrium at the point of achieving the minimum χ^2. Figure 6 illustrates the algorithmic flow of the equilibrium reconstruction process in KTX3DFit, providing a concise overview of the described procedure.

4.2. KTX3DFit equilibrium reconstruction results

This section primarily presents the content related to testing the reconstruction capability of KTX3DFit. A specific explanation regarding the reference signal ϕ_j^{ref} is provided here (tabel 1). Since 3D equilibrium program VMEC has been successfully applied to KTX [53], the ϕ_j^{ref} required in equation (9) is calculated based on the equilibrium results from the VMEC or SPEC (figure 8). For reconstructing the axisymmetric state and SHAx state, the ϕ_j^{ref} obtained from the VMEC equilibrium by scanning the q-profile [53], is denoted as ϕ_j^{vmec}. Meanwhile, for DAx states reconstruction, due to the unavailability of DAx state datas from VMEC, we set $\phi_j^{\mathrm{ref}} = \phi_j^{\mathrm{spec}}$, where ϕ_j^{spec} represents the polarimeter-interferometer signals of the DAx state obtained from SPEC (as refereced in section 3.2).

We employ a combination of $|\Delta\phi|$, poincare plots and q-profiles to demonstrate that our reconstructed magnetic field accurately identifies the corresponding self-organized states.

The fitting results of the Faraday rotation angle signals achieved by KTX3DFit, minimizing the χ^2 value, demonstrate a reasonable agreement with reference signals (figure 7). In the case of the DAx state (figure 7(e)), $|\Delta\phi|$ consistently falls below the error $\sigma_j = 0.8°$ [48], where $|\Delta\phi| = |\phi_j^{\mathrm{calculate}} - \phi_j^{\mathrm{ref}}|$ represents the absolute value of the difference for each channel. For the axisymmetric state and SHAx state (figures 7(d) and (f), although a few channels exhibit $|\Delta\phi| > \sigma$, the majority of channels have $|\Delta\phi|$ values within the range of the σ_j. From different toroidal positions, the $|\Delta\phi|$ in the axisymmetric state overlap, whereas $|\Delta\phi|$ in the DAx state and SHAx state oscillate across different toroidal directions. In other words, the $|\Delta\phi|$ response differs between the 2D axisymmetric state and the 3D QSH state.

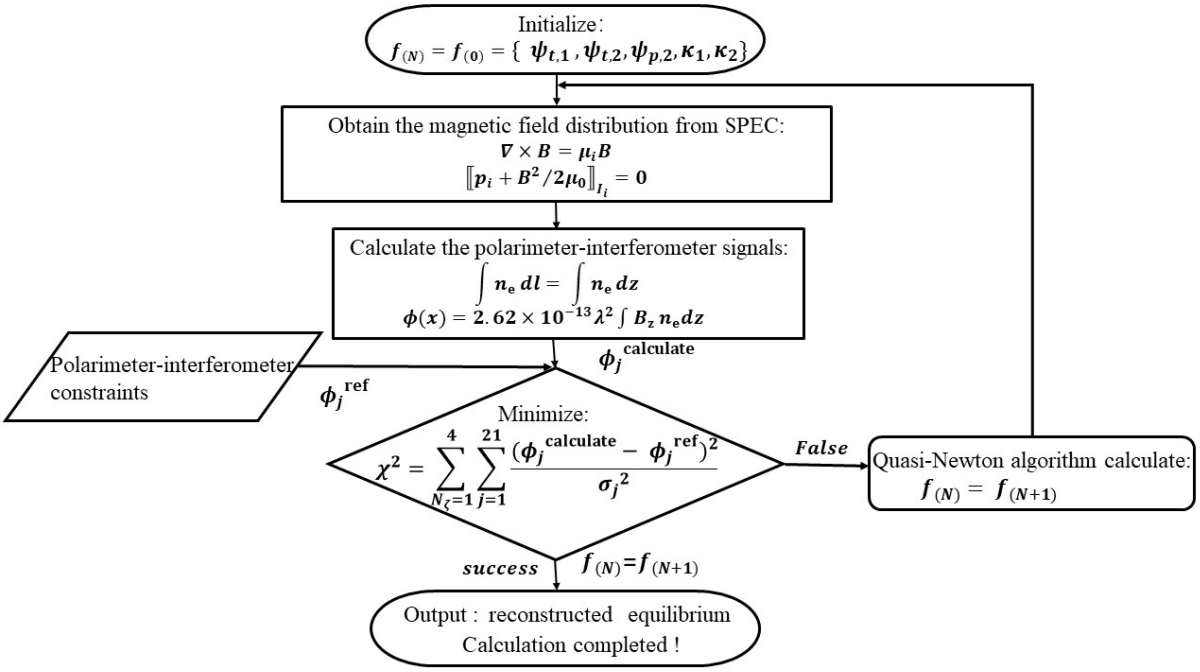

Figure 6. Flowchart of KTX3DFit equilibrium reconstruction algorithm.

Table 1. Reference signal ϕ_j^{ref} description.

Case	Reference signal
Axisymmetric state	ϕ_j^{vmec}
DAx state	ϕ_j^{spec}
SHAx state	ϕ_j^{vmec}

The magnetic fields of different self-organized states exhibit distinct magnetic topology structures, and the magnetic shear in the core region varies for these states [41], as reflected in the reconstruction results of this work. Figure 8 illustrates the magnetic topology structures and core q-profiles of the axisymmetric state, DAx state, and SHAx state reconstructed by KTX3DFit. The results show a high

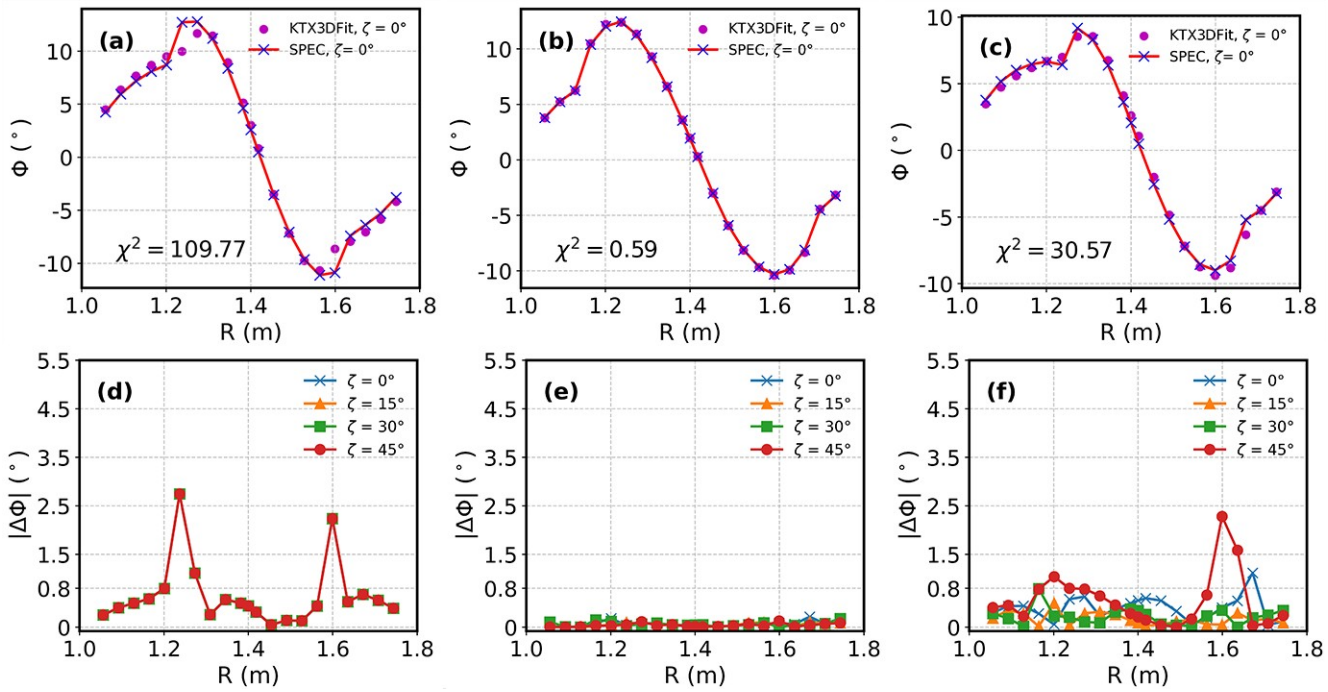

Figure 7. Comparison between Faraday rotation angle $\phi_j^{calculate}$ reconstructed by KTX3DFit and the reference signal for various self-organized states. (a), (d): Axisymmetric state. (b), (e): DAx state. (c), (f): SHAx state. (a), (b), and (c) show the comparison between $\phi_j^{calculate}$ and reference signal at $\zeta = 0°$. (d), (e), and (f) display the absolute differences at $\zeta = 0°$, 15°, 30°, 45°. In figures (a) and (c), $\phi_j^{ref} = \phi_j^{vemc}$, while in figure (b), $\phi_j^{ref} = \phi_j^{spec}$.

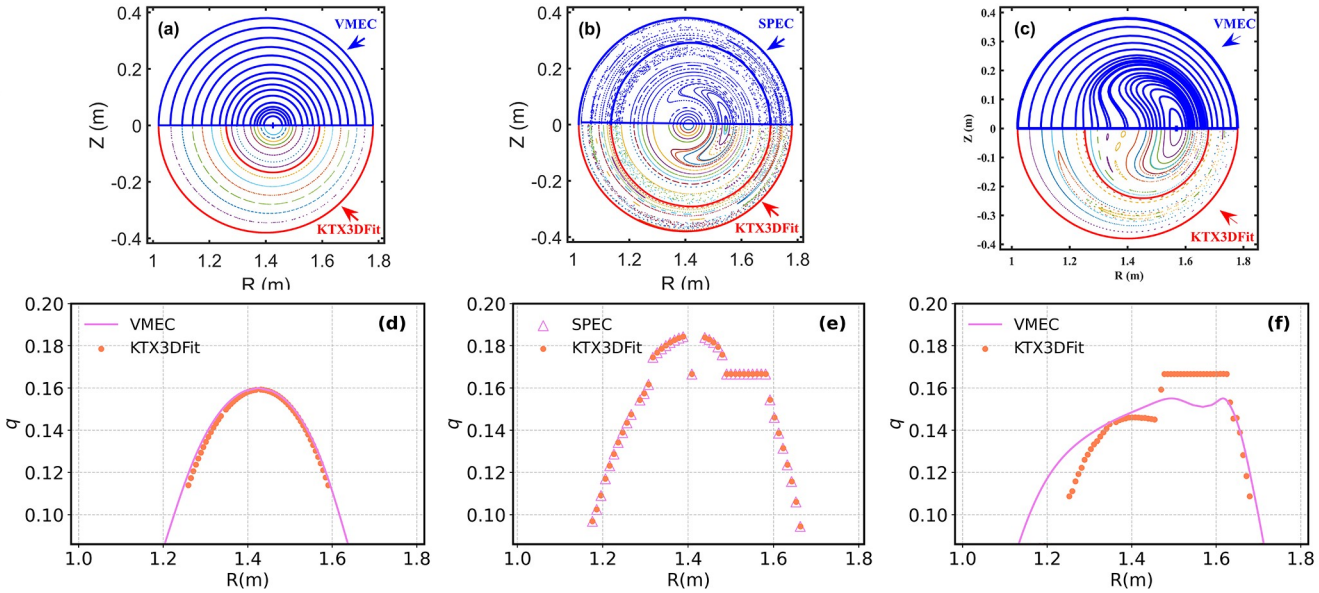

Figure 8. Comparison of the magnetic topology and core q-profiles reconstructed by KTX3DFit for different self-organized states with corresponding reference states. (a), (d): Axisymmetric state. (b), (e): DAx state. (c), (f): SHAx state. (a), (b), and (c) depict the magnetic topology. (d), (e), and (f) show the core q-profiles.

consistency with the reference states, indicating that the reconstructed equilibria and those reference states correspond to the same type of self-organized state. In the axisymmetric state (figure 8(d), the q-profile demonstrates a monotonic decrease on both sides of the magnetic axis. For the QSH state (figures 8(e) and (f)), the magnetic shear near the bean-shaped magnetic island in the core region tends toward zero. The presented q-profile results of the self-organized states agree with experimental observations made on RFX-mod [41]. Moreover, in this reconstruction work, the core q-profile under the DAx state aligns most closely with reference profile, both originating from the SPEC numerical solver. In the SHAx state, inherent differences in the SPEC and VMEC, along with the influence of transport barriers and small magnetic islands near the core bean-shaped magnetic island, result in a slightly lower agreement between the two datasets in figure 8(c) compared to the axisymmetric state. The results demonstrate that KTX3DFit is able to reconstruct various equilibria with different self-organized states.

5. Discussion and summary

In the framework of the MRxMHD model, we utilize the SPEC program and employ a transport barrier to partition the plasma into two regions. By adjusting the helicity in each subregion, we have successfully simulated the different self-organized states in KTX.

Simulation of polarimeter-interferometer signals in KTX indicates distinct responses to different plasma states. Therefore, utilizing these signals for various states reconstruction is theoretically feasible. From the same toroidal position, variations in polarimeter-interferometer signals among different states are noticeable. When inspecting different toroidal positions, signals under the axisymmetric state overlap, whereas under the DAx and SHAx states, distinct signals are observed, with the disparities being more pronounced under the SHAx state. Simulated temporal signals under different self-organized states exhibit similar characteristics. From the above, it can be seen that polarimeter-interferometer signals can accurately distinguish between the 2D and 3D structures of the plasma.

The developed 3D equilibrium reconstruction program, KTX3DFit, successfully reconstructs axisymmetric state, DAx state, and SHAx state in the KTX configuration. The results show typical magnetic topology structures for each self-organized state, and q-profiles are consistent with the reference data. The reconstructed Faraday rotation angles fit well with the reference signals. Simulated errors in polarimeter-interferometer signals on most channels are within the noise level of the installed polarimeter-interferometer on KTX.

The development of KTX3DFit provides a strategy for reconstructing 3D plasma equilibrium with chaos and magnetic islands. This study focuses on testing the feasibility of the new code. Although experimental measurements are not employed here, the process, which is based on reference states known magnetic topology information, is reasonable. This helps us assess whether the equilibrium reconstructed by KTX3DFit aligns with the reference state. In future work, we intend to incorporate experimental measurements (including both polarimeter and interferometer) to enhance KTX3DFit robustness, and assess its performance. Furthermore, the positions and numbers of polarimeter-interferometer channels on KTX can be optimized to maximize space efficiency, while studying the impact of measurement precision for equilibrium reconstruction. Moreover, other diagnostic tools can be integrated into KTX3DFit.

Acknowledgments

This work was supported by National Natural Science Foundation of China (Nos. 12175227 and 12375226), the National Magnetic Confinement Fusion Program of China (No. 2022YFE03100004), the Fundamental Research Funds for the Central Universities (No. USTC 20210079), and the Collaborative Innovation Program of Hefei Science Center, CAS (No. 2022HSC-CIP022).

References

[1] Callen J D 2011 *Nucl. Fusion* **51** 094026
[2] Cooper W A *et al* 2010 *Phys. Rev. Lett.* **105** 035003
[3] Jiang Z H *et al* 2022 *Plasma Sci. Technol.* **24** 124014
[4] Lorenzini R *et al* 2009 *Nat. Phys.* **5** 570
[5] Escande D F *et al* 2000 *Plasma Phys. Control. Fusion* **42** B243
[6] Escande D F *et al* 2000 *Phys. Rev. Lett.* **85** 1662
[7] Fitzpatrick R 2024 *Phys. Plasmas* **31** 042510
[8] Escande D F *et al* 2000 *Phys. Rev. Lett.* **85** 3169
[9] Biewer T M *et al* 2003 *Phys. Rev. Lett.* **91** 045004
[10] Zanca P *et al* 2001 *Phys. Plasmas* **8** 516
[11] Lorenzini R *et al* 2008 *Phys. Rev. Lett.* **101** 025005
[12] Lorenzini R *et al* 2009 *Phys. Plasmas* **16** 056109
[13] Terranova D *et al* 2010 *Nucl. Fusion* **50** 035006
[14] Lao L L *et al* 1990 *Nucl. Fusion* **30** 1035
[15] Lao L L *et al* 1985 *Nucl. Fusion* **25** 1611
[16] McCarthy P J 1999 *Phys. Plasmas* **6** 3554
[17] Moret J M *et al* 2015 *Fusion Eng. Des.* **91** 1
[18] Faugeras B 2020 *Fusion Eng. Des.* **160** 112020
[19] Hirshman S P and Whitson J C 1983 *Phys. Fluids* **26** 3553
[20] Hirshman S P, Van Rij W I and Merkel P 1986 *Comput. Phys. Commun.* **43** 143
[21] Hanson J D *et al* 2009 *Nucl. Fusion* **49** 075031
[22] Terranova D *et al* 2010 *Contrib. Plasma Phys.* **50** 775
[23] Suzuki Y, Nakamura Y and Kondo K 2003 *Nucl. Fusion* **43** 406
[24] Martines E *et al* 2011 *Plasma Phys. Control. Fusion* **53** 035015
[25] Auriemma F *et al* 2011 *Plasma Phys. Control. Fusion* **53** 105006
[26] Newcomb W A 1960 *Ann. Phys.* **10** 232
[27] Zanca P and Terranova D 2004 *Plasma Phys. Control. Fusion* **46** 1115
[28] Hudson S R and Dewar R L 2012 *Phys. Plasmas* **19** 112502
[29] Hole M J, Hudson S R and Dewar R L 2007 *Nucl. Fusion* **47** 746
[30] Hudson S R, Hole M J and Dewar R L 2007 *Phys. Plasmas* **14** 052505
[31] Taylor J B 1986 *Rev. Mod. Phys.* **58** 741
[32] Taylor J B 1974 *Phys. Rev. Lett.* **33** 1139
[33] Dennis G R *et al* 2013 *Phys. Rev. Lett.* **111** 055003
[34] Liu K *et al* 2024 *Nucl. Fusion* **64** 056037
[35] Dodel G and Kunz W 1978 *Infrared Phys.* **18** 773
[36] Wang Y H *et al* 2022 *Plasma Sci. Technol.* **24** 064001
[37] Zhang J *et al* 2013 *Plasma Phys. Control. Fusion* **55** 045011
[38] Dewar R L *et al* 2015 *J. Plasma Phys.* **81** 515810604
[39] Dennis G R *et al* 2013 *Phys. Plasmas* **20** 032509
[40] Kumar A *et al* 2021 *Plasma Phys. Control. Fusion* **63** 045006
[41] Gobbin M *et al* 2011 *Phys. Rev. Lett.* **106** 025001
[42] Brower D L *et al* 2002 *Phys. Rev. Lett.* **88** 185005
[43] Loizu J, Hudson S R and Nührenberg C 2016 *Phys. Plasmas* **23** 112505
[44] Imbert-Gerard L M, Paul E J and Wright A M 2019 *arXiv e-prints* **arXiv:** 1908.05360
[45] Liu J *et al* 2021 *Nucl. Fusion* **61** 016017
[46] Brower D L *et al* 2001 *Rev. Sci. Instrum.* **72** 1077
[47] Chen J *et al* 2016 *Rev. Sci. Instrum.* **87** 11E108
[48] Wang X K *et al* 2024 *Plasma Sci. Technol.* **26** 034009
[49] Joshi N Y, Atrey P K and Pathak S K 2010 *J. Phys.: Conf. Ser.* **208** 012129
[50] Frassinetti L *et al* 2006 *Phys. Rev. Lett.* **97** 175001
[51] Mao W Z *et al* 2021 *Rev. Sci. Instrum.* **92** 053514
[52] Tarantola A 2005 *Inverse Problem Theory and Methods for Model Parameter Estimation* (Philadelphia: SIAM)
[53] Zu Y M *et al* 2022 *Plasma Phys. Control. Fusion* **64** 065002